Pergamon

Int. J. Heat Mass Transfer. Vol. 39, No. 14, pp. 2861–2867, 1996

0017-9310/96 $15.00 + 0.00

0017-9310(95)00372-X

Pore formation in hot spots

I. H. KATZAROV and J. R. POPOV

Institute for Metal Science, Bulgarian Academy of Sciences, 67 Shipchenski Prohod str., 1574 Sofia, Bulgaria

(*Received for publication* 7 *November* 1995)

Abstract—In previous works we have introduced the basic features of a method for the numerical simulation of heat and mass transfer processes during casting formation. Within this approach we describe here the evolution of pressure and the formation of porosity defects in hot spots by the simultaneous treatment of thermoelastic, crystallization and porosity growth problems in axially symmetric castings. Copyright © 1996 Elsevier Science Ltd.

1. INTRODUCTION

The porosity may result from shrinkage, dissolved gases, or a combination of both, and may take the form of either macroscopic pores in localized area or microporosity, evenly distributed throughout large areas in the casting. The interdendritic porosity (microporosity) arises because the solubility of hydrogen is less in the solid than in the liquid metal, so that some of the hydrogen is expelled into the interdendritic liquid. Thus, the concentration of the dissolved hydrogen, and therefore its partial pressure rises with the progress of solidification. If the concentration of hydrogen in the interdendritic liquid rises to a value sufficient to exceed the sum of the local pressure in the interdendritic liquid and the excessive pressure attributed to surface tension, then microporosity appears. The shrinkage porosity is caused by the inefficiency of the feeding mechanism, which supplies molten metal to the solidification front. The resistance to filtration flow causes a pressure drop across the dendritic network. The formation of shrinkage porosity and gas holes at separate locations is rare, and usually both processes—pressure drop due to filtration, and partial pressure increase of the dissolved gas—occur simultaneously at the same place.

There are reports of computer simulations of porosity formation, accounting for the shrinkage and dissolved gas evolution, in castings with a permanent feeding of the two-phase region with molten metal [1–4]. A different pattern of porosity formation is realized when the molten metal is enclosed in a solid shell and the feeding is ceased (hot spot). In this case, the porosity defects result from the shrinkage in the two-phase region, the content of dissolved gases in the hot spot, and the thermal contraction due to the progress of crystallization in the outer layers. In ref. [5] we obtained the deformations, stresses and strains in the casting–mould system within a linear thermoelastic model, and described the evolution of the air gap and its influence on the process of crystallization. We demonstrated a solution for the same configuration without a feed up of the two-phase region, i.e. when the molten metal remains enclosed in the solid shell. Then the pressure in the hot spot changes during the process—in the case considered in ref. [5] it rises initially, because the outer layers are shrinking (ρ is considered to be constant during the phase transition) and afterwards, when the crystallization takes place in the considered volume the pressure falls to zero. It becomes feasible, in this context, to describe the local phenonemena which influence the metal microstructure during crystallization.

The research reported here extends this model to include the effects of volume contraction in the two-phase region. The change of the density ρ during the phase transition is compensated for by the growth of porosity. The pressure in the molten metal provides the boundary conditions, which are needed to treat the formation of porosity defects, and in its turn is determined from the balance between the volume contraction due to the crystallization in the outer layers and the shrinkage in the mushy zone, compensated for by interdendritic flow. The aim of the present research is to describe the creation of porosity defects in hot spots by simultaneous treatment of thermoelastic, crystallization, shrinkage and gas evolution in the two-phase region in axially symmetric castings.

2. MATHEMATICAL MODELING

2.1. *Heat balance equation*

In previous papers by the same authors [6, 5] we proposed a new model for simultaneous treatment of hydrodynamic cooling and crystallization problems in castings with complex shapes. Within this approach, an irregular shaped physical domain is mapped into a computational domain with a regular geometry, where well developed finite difference techniques can be applied. The equations of heat and mass transfer are written and numerically solved in a

NOMENCLATURE

c	heat capacity coefficient
d	primary dendrite arm spacing
F	density of the external volume
f_L, f_S, f_P	volume fractions of liquid, solid and pore phases
$[H_0]$	initial hydrogen content in the liquid metal
$[H_L], [H_S]$	hydrogen concentration in liquid and solid
k	segregation coefficient
k_0	permeability in the mushy region
K_{LH}, K_{SH}	equilibrium constants for hydrogen in liquid and solid metal
L	latent heat of crystallization
P	interdendritic liquid pressure
P_g	gas pressure
P_M	liquid pressure in the molten metal
$\mathbf{q}$	heat flux vector
t	time
$\mathbf{t}^{ij}$	stress tensor
T	temperature
T_m	melting point of pure metal
T_L	liquidus temperature
u	velocity
W	density of the internal energy.

Greek symbols

α_H	constant in equation (8) $27\,300/(f_L\rho_L+f_S\rho_S)$
β	thermal expansion coefficient
Γ^i_{jk}	affine connection coefficients
θ^{ij}	velocity of deformation tensor
κ	heat conductivity coefficient
λ, μ	Lame's coefficients
ν	viscosity of liquid
ρ	specific density
ρ_S, ρ_L	densities of solid and liquid
σ	liquid–gas surface tension.

coordinate space R, obtained through a metric mapping from the space of the real process. The mapping is constructed in such a way, that a boundary fitted coordinate system is obtained. The coordinate system is generated by algebraic methods, which makes more feasible the problem of its updating in cases with non-stationary metric. The equations of heat and mass transfer in the boundary fitted coordinate system with metric tensor $\mathbf{G}_{ab}$ should be derived in a covariant way in order to account for the effects of boundary curvature and nonstationarity. We obtain them from the laws of conservation of mass, momentum and energy, defined in the coordinate space R. The corresponding equations are:

(a) mass

$$(1/\sqrt{\mathbf{G}})\,\partial_t(\sqrt{\mathbf{G}}\rho)+\nabla\cdot(\rho u)=0 \tag{1}$$

(b) momentum

$$\rho(u^i_{,t}+u^k\nabla_k u^i+2\Gamma^i_{jk}u^k)-\nabla_k t'^k=\rho F^i \tag{2}$$

(c) energy

$$\rho(W_{,t}+W\,\partial_t\ln\mathbf{G}+u^iW_{,i})=t_{ij}\theta^{ij}-\nabla_i\mathbf{q}^i+\rho u^kF_k. \tag{3}$$

The heat problem is solved in two regions, with solid and molten metal, where the equation is

$$\rho(c+L\,\partial_T f_S)\,\partial_t T=\nabla\kappa\cdot\nabla T. \tag{4}$$

The boundary conditions of I and III kind follow from $\partial_n T=\mathbf{N}\cdot\nabla T$, where the vector $\mathbf{N}$ is normal to the boundary surface. The crystallization is described by the method of equivalent heat capacity $c_E=c-L\,\partial_T f_S$, where the relationship between solid fraction f_S and temperature T is obtained by the Sheil expression

$$f_S=1-\left(\frac{T-T_m}{T_L-T_m}\right)^{\frac{1}{k-1}}$$

2.2. *Formation of porosity*

It is assumed that a gas pore is stable provided that the excess pressure in the gas is sufficient to overcome the surface tension, while the gas phase has a radius that is small enough to fit in the interdendritic space. Since the primary dendrite spacing is at least an order of magnitude higher than the secondary dendrite arm spacing, the surface tension barrier to be overcome for the formation of gas pore within the secondary spacing would be much higher. The above requirements are expressed as

$$P_g-P=\frac{4\sigma}{d}. \tag{5}$$

While porosity has not formed the local pressure in the two-phase region P is calculated from the continuity equation

$$\left(\frac{\rho_S}{\rho_L}-1\right)\frac{\partial f_L}{\partial t}-\nabla\cdot(f_L u)+\frac{\partial f_P}{\partial t}=0, \tag{6}$$

through the equation describing interdendritic flow (Darcy's law)

$$u=-\frac{k_0}{\nu f_L}\nabla\cdot P. \tag{7}$$

Equation (6) indicates that the shrinkage during the

solidification (first term) is compensated by interdendritic flow (second term) and the growth of porosity (the last term). The permeability k_0 in the Darcy's law can be expressed by the Blake–Kozeney equation [3] as

$$k_0 = \frac{f_L^3 d^2}{180(1-f_L)^2}.$$

The primary dendrite arm spacing d is inversely proportional to the local temperature gradient G_L and the solidification growth velocity u_S and can be expressed as [7]

$$d = aG_L^{-b}u_S^{-c}$$

where a, b, c are constants.

P_g is calculated from equation (5). A new amount of porosity is obtained from the conservation equation for gas content

$$[H_0] = (1-f_L)[H_S] + f_L[H_L] + \alpha_H \frac{P_g f_P}{T}. \quad (8)$$

The left side is the initial hydrogen content. The first, second and third terms on the right are the amounts of hydrogen in the solid, liquid and porosity, respectively. It is sufficient to consider only the hydrogen as a contributor to microporosity in aluminum alloys because it is the only gas with a measurable solubility in aluminum. The hydrogen contents in the solid and liquid are expressed by the Sievert's law as

$$[H_S] = K_{SH}P_g^{1/2}$$

$$[H_L] = K_{LH}P_g^{1/2}$$

The procedure described above is repeated over each volume element in the two-phase region and at each time step, until the required time is reached. The equations (6) and (7) are solved jointly with the problem for cooling and crystallization (4) with initial and boundary conditions settled above. The interaction between the heat and pore formation problems takes place through the mushy zone which is updated at each time step. Equations (6) and (7) are solved by a finite difference method in a local orthogonal coordinate system fitted to the boundaries of the two-phase region. The coordinate surfaces are the isotherms $T(\eta) = \text{const}$ and the integral lines $x(\zeta)$ of the temperature gradient, which are obtained from the system of ordinary differential equations

$$\frac{dx^i}{d\zeta} = \nabla_i T(x(\zeta)). \quad (9)$$

The system (9) provides the transition functions between the coordinates $\{x^i\}$ in the coordinate space R and the local coordinates $\{\eta, \zeta\}$ in the two-phase region. Since the geometry of the mushy zone is nonstationary, the local coordinate system is updated at each time step.

The boundary conditions in the mushy region are set as follows. At the centerline and at the mould wall of an axi-symmetric casting, i.e. where $r = 0$ and $r = r_a$ (r_a is the casting radius)

$$u_r = 0; \quad \frac{\partial P}{\partial r} = 0$$

where $u_r = r$-component of the velocity. Along the liquidus isotherm, the pressure is equal to the pressure in the molten metal P_M, which is obtained after simultaneous treatment of porosity formation and thermoelastic problems in the case of hot spot. When the molten metal is not enclosed within a solid shell, we assume that the pressure is atmospheric. At the liquidus isotherm liquid metal flows to feed the shrinkage

$$u_\zeta = -\left(\frac{\rho_S}{\rho_L} - 1\right)u_L$$

where u_L is the liquidus isotherm velocity.

2.3. *The thermoelastic model*

The equations for stresses and deformations are derived from the corresponding laws of conservation in the Riemannian space R. We use a linear model defined by the stress tensor

$$\mathbf{t}^{ik} = A(T)G^{ik}\delta T + B(T)(\nabla\cdot\xi)G^{ik} + C(T)(\nabla^i\xi^k + \nabla^k\xi^i). \quad (10)$$

The coefficients A, B and C are obtained on the assumption of adiabatic initial conditions

$$A = \Lambda\beta/(1+Z\Lambda); \quad B = \lambda - Z\Lambda^2/(1+Z\Lambda); \quad C = \mu$$

where $Z = T_0\beta^2/c$; $\Lambda = \lambda + 2/3\mu$.

With the use of the expression $G^{ij}\Gamma^k_{jl} + G^{ik}\Gamma^i_{jl} = -G^{ik}_{,l}$, the stress tensor is written down in partial derivatives

$$\mathbf{t}^{ik} = AG^{ik}\delta T + BG^{ik}(\xi^l_{,l} + (\ln\sqrt{\mathbf{G}})_{,l}\xi^l) + C(G^{il}\xi^k_{,l} + G^{kl}\xi^i_{,l} - G^{ik}_{,l}\xi^l) \quad (11)$$

In the case when the inertia and convective terms can be neglected, equation (2) is presented in the form

$$\rho F^i + 2\rho\Gamma^i_{ik}\xi^k_{,t} = \nabla_k\mathbf{t}^{ik} = AG^{ki}\nabla_k\delta T + (B+C)G^{ki}\nabla_k\nabla_i\xi^i + C\Delta\xi^i + C\mathbf{R}^i_k\xi^k \quad (12)$$

where $\mathbf{R}_{ik}$ is the curvature tensor of a coordinate surface S [5].

The boundary conditions for equation (12) vary during the process. The components of the normal stress on a surface S will be

$$P^i = \mathbf{t}^i_j N^j = (A\delta T + B(\xi^l_{,l} + (\ln\sqrt{\mathbf{G}})_{,l}\xi^l))N^i + C(G^{il}G_{kn}\xi^n_{,l} + \xi^i_{,k} + G^{ij}_{,l}G_{jk}\xi^l)N^k. \quad (13)$$

Initially the normal stress on the walls of the form $P = P^i\mathbf{N}_i$ equals the initial pressure. After a crust is formed, it diminishes because of the shrinkage. While

$P > 0$, the boundary conditions are $\xi_S^i = 0$. When P becomes zero, the boundary conditions are determined from the expression $P = 0$. The air gap, which appears, is determined as the sum of the boundary displacements of the casting and mould

$$\delta(t) = \xi(t) \cdot \mathbf{N}_{|C} + \xi(t) \cdot \mathbf{N}_{|M}.$$

In this case the heat transfer between the mould and the casting will change significantly.

2.4. *Pressure evolution in the hot spot*

The system of equations (4) and (12), written in the coordinate space R, is solved jointly with the problem for pore formation (6)–(8) with the initial and boundary conditions settled above. The interactions between the pore formation and the mechanical problems take place through the boundary conditions: the pressure P_M in the molten metal provides a boundary condition for the continuity equation (6). In ref. [5] we demonstrated a solution for the isotropic part of stress tensor in the case when the molten metal remains enclosed after the formation of solid core.

$$\tfrac{1}{3}Trt = B(T)(\nabla \cdot \xi) \tag{14}$$

without taking into account the shrinkage of the two phase region and pore formation. The pressure change ΔP_M for a moment Δt can be obtained from equation (14) in the form

$$\Delta P_M = B(T)\frac{\Delta V_{EL}}{V},$$

where V is the volume enclosed by the solid crust and ΔV_{EL}, is the volume contraction which occurs because of the shrinkage of the outer layers.

From the mass balance equation (6) the shrinkage during the solidification in V can be obtained

$$\Delta V_S = \int_v \left(\frac{\rho_S}{\rho_L} - 1\right)\frac{\partial f_L}{\partial t}\,dv$$

compensated by interdendritic flow and the growth of porosity

$$\Delta V_P = \int_v \frac{\partial f_P}{\partial t}\,dv.$$

$\Delta V_S - \Delta V_P$ is the volume contraction in the area enclosed within the solid core, which has to compensate for the contraction ΔV_{EL} resulting from the shrinkage of the outer layers. In the case when $\Delta V_{EL} < \Delta V_S$, the pressure in the molten metal is calculated from the volume balance equation

$$\Delta V_S - \Delta V_{EL} = \Delta V_P \tag{15}$$

by an iterative procedure. When $\Delta V_{EL} > \Delta V_S$ the pressure P_M is obtained as

$$P_M = P_0 + \Delta P$$

where P_0 is the pressure for which porosity growth is zero and

$$\Delta P = B(T)\frac{\Delta V_{EL} - \Delta V_S}{V}$$

(we do not take into consideration such problems as plastic deformations, stress relaxation and distortions of the dendritic network).

3. RESULTS AND DISCUSSION

The system of differential equations (4), (6)–(8) and (12) in the case of the hot spot was solved numerically for an axi-symmetric casting-mould system. Calculations were carried out for an alloy with parameters listed in Table 1. In Fig. 1 we present the distribution of the amount of porosity. The calculated radius of the porosity is shown in Fig. 3. The evolution of the pressure in the molten metal is presented in Fig. 4. The pressure remains atmospheric up to the enclosing of the molten metal within the solid crust. As the solid crust is formed, the pressure drops sharply and the porosity growth increases accordingly in order to compensate for the shrinkage solidification [Fig. 1(a)]. With the progress of crystallization the pressure in the molten metal consequently rises, because the outer layers are shrinking and the amount of porosity decreases following equation (15) [Fig. 1(b)]. When molten metal in enclosed within the solid shell, the feeding is ceased and the mass deficit is calculated from the mass balance for the volume element equation (6) [Fig. 1(c)]. In this case even very small stresses will cause separation of the interdenritic liquid films. The separation of these liquid films causes the appearance of hot cracking. In Fig. 2 we demonstrate another solution for the same configuration, this time without taking into account the thermomechanical effects and assuming that the pressure in the molten metal is atmospheric during the process. The calculated change of amount and distribution of porosity indicates that the thermomechanical effects can not be

Table 1. Parameter values

c	1088 J.kg^{-1}.grad^{-1}
$[H_0]$	0.2 cc/100 g
k	0.173
K_{LH}	0.6 cc/100 g.atm$^{1/2}$
K_{SH}	0.06 cc/100 g.atm$^{1/2}$
L	4×10^5 J.kg^{-1}
T_m	660°C
T_l	645°C
β	$\beta_0 + \beta_1 T$; $\beta_0 = 0.7 \times 10^{-4}$; $\beta_1 = 10^{-8}$ grad^{-1}
κ	200 W.m^{-1}.grad^{-1}
λ	0.49×10^{11} N.m^{-2}
μ	$\mu_0 + \mu_1 T + \mu_2 T^2$; $\mu_0 = 0.25 \times 10^{11}$ N.m^{-2}; $\mu_1 = 0.246 \times 10^3$ N.m^{-2}.grad^{-1}; $\mu_2 = 0.25 \times 10^5$ N.m^{-2}.grad^{-2}
ρ_S	2520 kg.m^{-3}
ρ_L	2380 kg.m^{-3}

(a)

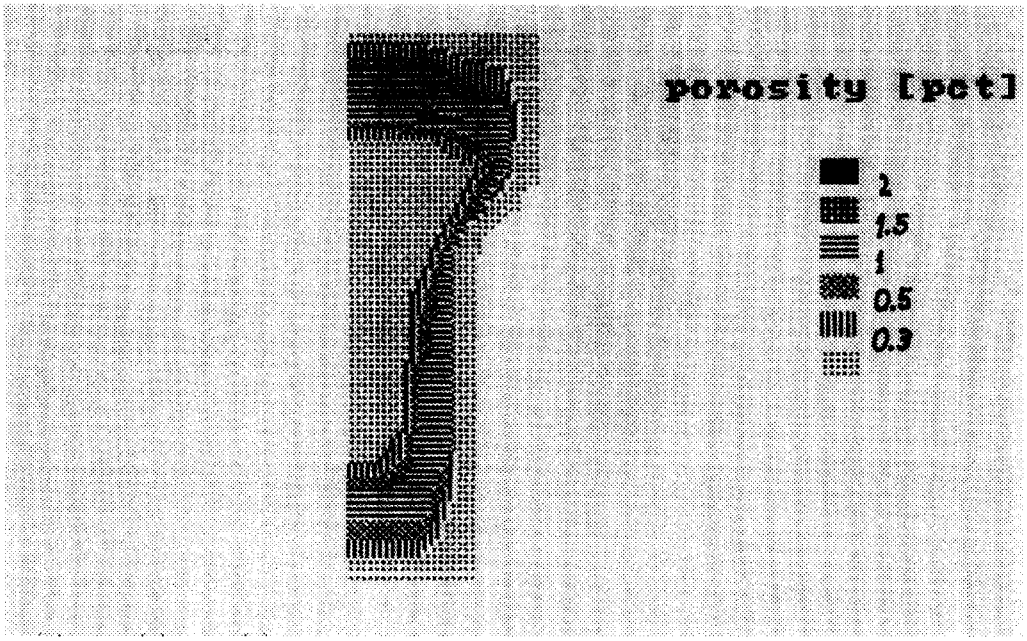

(b)

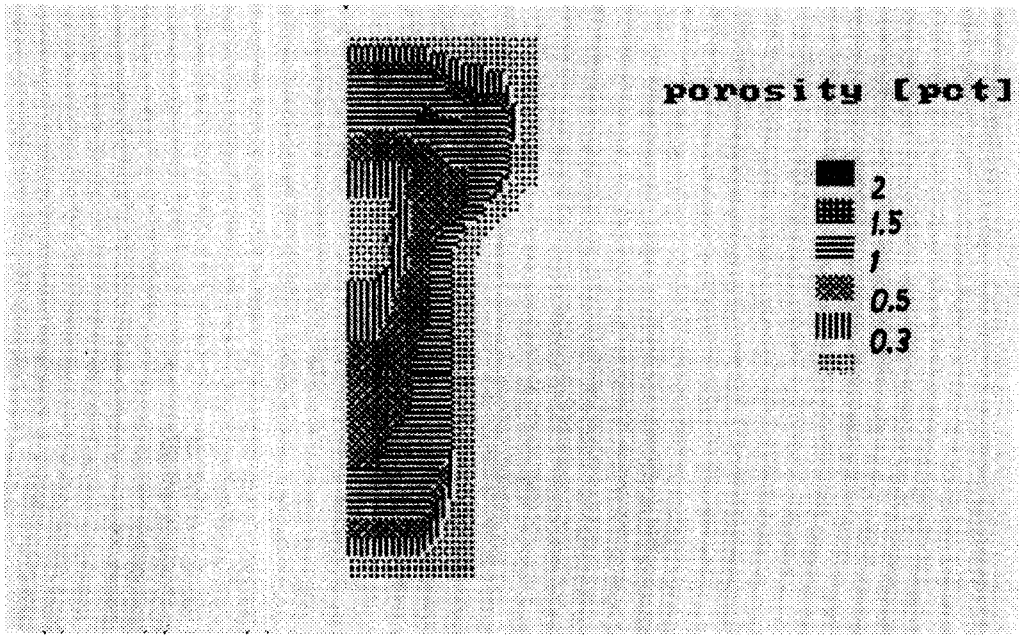

Fig. 1. Three successive positions of the solidification front in a casting with a 'hot spot'. (a) At the beginning of the crystallization the pressure inside the casting is low, because the overall volume of the phase transition zone is large, while the solid shell is thin. The percentage of pores is relatively high. (b) When the solidification advances inside the casting, the ratio between the volume of the two-phase zone and the solid shell decreases, and the pressure of the liquid metal rises, cf. Fig. 4. The pore content in the zone diminishes. (c) At the end of crystallization process, the volume deficit is so large, that it can not be compensated for by the poor growth; a cavity is formed around the centerline of the casting. The mathematical model used in this article does not allow us to describe the processes at this stage of crystallization. (*Continued overleaf.*)

(c)

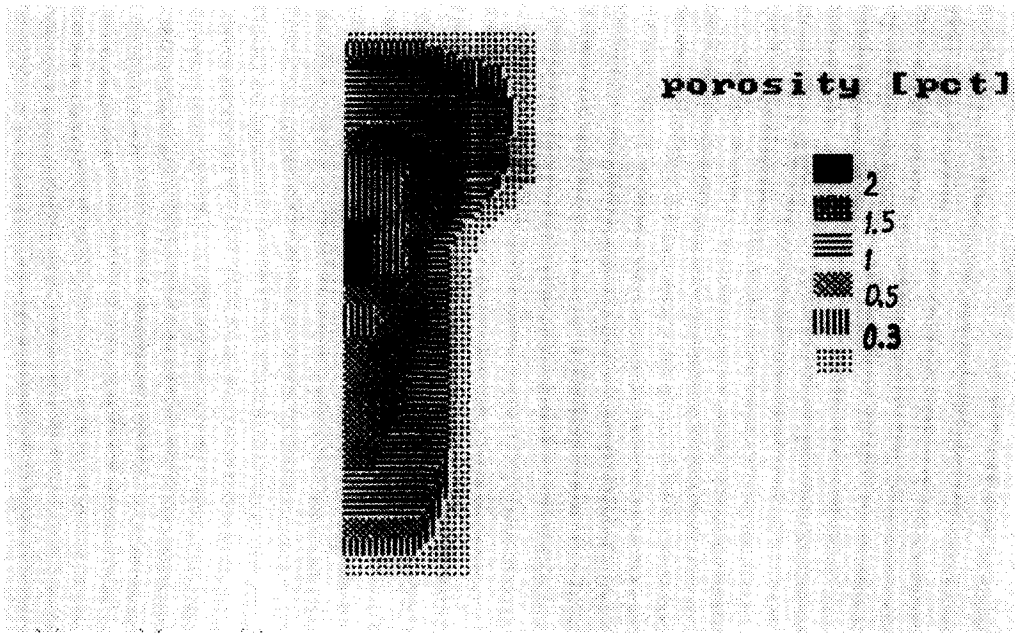

Fig. 1—*continued.*

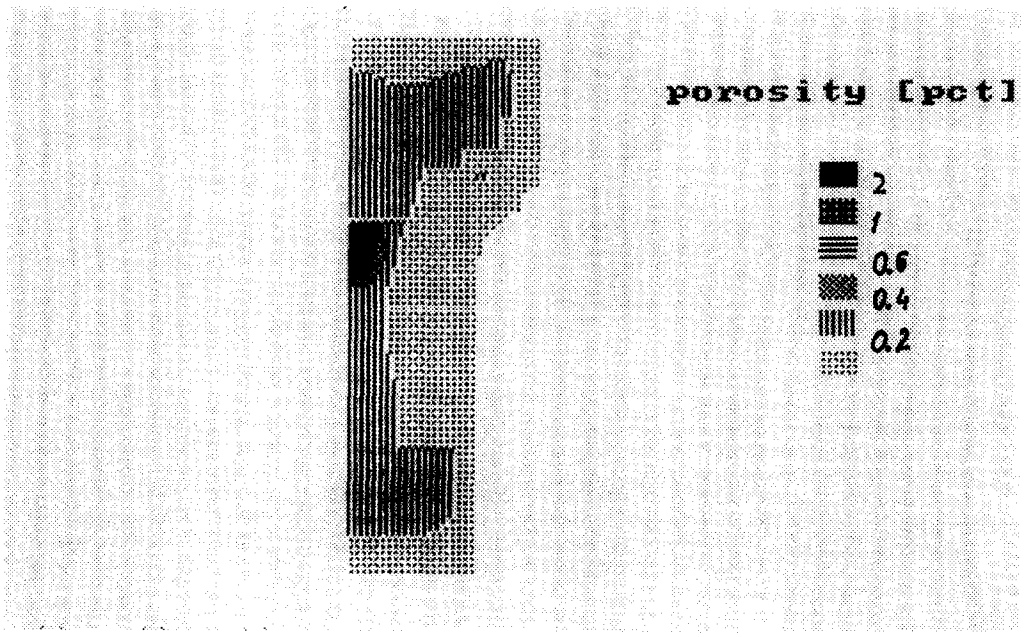

Fig. 2. The figure shows the pore distribution in a casting at the end of crystallization, when the pressure inside the melt is sustained at the permanent level of 1 atm.

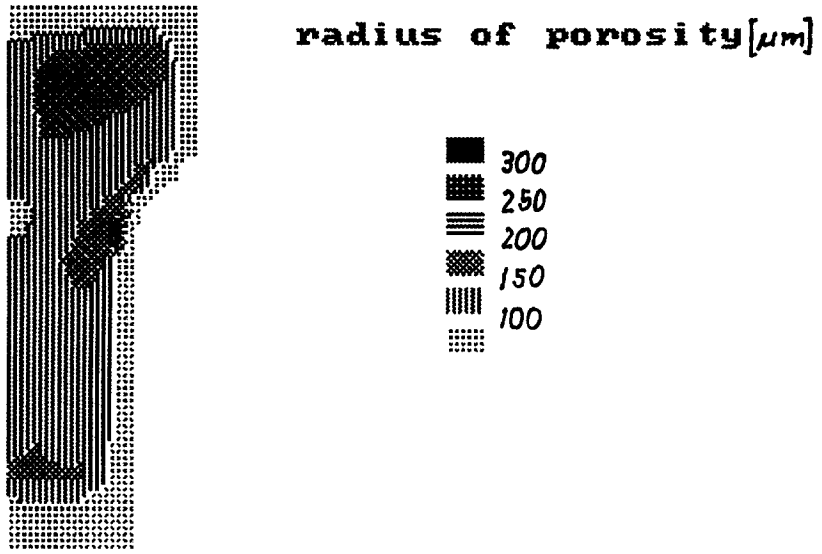

Fig. 3. The pore sizes, when crystallization follows the 'hot spot' pattern, described in Fig. 1.

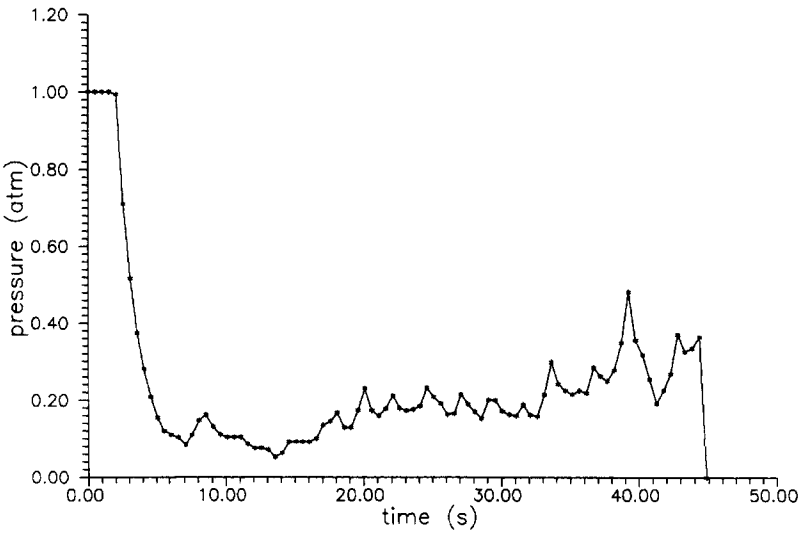

Fig. 4. Shows the pressure evolution with time inside the melt in the case of 'hot spot' type crystallization.

neglected and the problem for porosity formation in a hot spot can be solved only by simultaneous treatment of thermoeleastic, crystallization and porosity growth problems.

Acknowledgements—This work was partially supported by the National Science Foundation of Bulgaria under contract no. TH-236/1992.

REFERENCES

1. T. S. Piwonka and M. C. Flemings, *Trans. Met Soc. AIME* **236,** 1157 (1966).
2. K. Kubo and R. Pehlke, *Metall. Trans. B* **16,** 359 (1985).
3. D. R. Poirier, *Metal. Trans. B* **18,** 245–255 (1987).
4. V. K. Suri and A. J. Paul, *Micro Macro Scale Phenomena in Solidification*, HTD Vol. 218/AMD Vol. 139. ASME (1992).
5. J. R. Popov and I. H. Katzarov, *Int. J. Heat Mass Transfer*, **36,** 2861–2867 (1993).
6. J. R. Popov and I. H. Katzarov, *Int. J. Heat. Technol.* **8,** 60 (1990).
7. W. Kurz and D. J. Fisher, Trans. Tech. Publ., Aedermannsdorf, Switzerland, 85–87 (1986).
8. D. R. Poirier, K. Yeum and A. L. Maples, *Metall. Trans. A*, **18,** 1979 (1987).